Unmixing-Based Fusion of Hyperspatial and Hyperspectral Airborne Imagery for Early Detection of Vegetation Stress

Stephanie Delalieux, Pablo J. Zarco-Tejada, Laurent Tits, Miguel Ángel Jiménez Bello, Diego S. Intrigliolo, and Ben Somers

***Abstract*—Many applications require a timely acquisition of high spatial and spectral resolution remote sensing data. This is often not achievable since spaceborne remote sensing instruments face a tradeoff between spatial and spectral resolution, while airborne sensors mounted on a manned aircraft are too expensive to acquire a high temporal resolution. This gap between information needs and data availability inspires research on using Remotely Piloted Aircraft Systems (RPAS) to capture the desired high spectral and spatial information, furthermore providing temporal flexibility. Present hyperspectral imagers on board lightweight RPAS are still rare, due to the operational complexity, sensor weight, and instability. This paper looks into the use of a hyperspectral–hyperspatial fusion technique for an improved biophysical parameter retrieval and physiological assessment in agricultural crops. First, a biophysical parameter extraction study is performed on a simulated citrus orchard. Subsequently, the unmixing-based fusion is applied on a real test case in commercial citrus orchards with discontinuous canopies, in which a more efficient and accurate estimation of water stress is achieved by fusing thermal hyperspatial and hyperspectral (APEX) imagery. Narrowband reflectance indices that have proven their effectiveness as previsual indicators of water stress, such as the Photochemical Reflectance Index (PRI), show a significant increase in tree water-stress detection when applied on the fused dataset compared to the original hyperspectral APEX dataset ($R^2 = 0.62$, $p < 0.001$ vs. $R^2 = 0.21$, $p > 0.1$). Maximal R^2 values of 0.93 and 0.86 are obtained by a linear relationship between the vegetation index and the resp., water and chlorophyll, parameter content maps.**

***Index Terms*—Citrus, fusion, hyperspatial, hyperspectral, thermal, unmixing, water stress.**

Manuscript received September 23, 2013; revised March 24, 2014; accepted June 01, 2014. Date of publication July 07, 2014; date of current version August 01, 2014. This work was supported in part by the Belgian Science Policy Office in the frame of the Stereo II program (Hypermix project—SR/00/141), in part by the project Chameleon of the Flemish Agency for Innovation by Science and Technology (IWT), and in part by the Spanish Ministry of Science and Education (MEC) for the projects AGL2012-40053-C03-01 and CONSOLIDER RIDECO (CSD2006-67). The European Facility for Airborne Research EUFAR (www.eufar.net) funded the flight campaign (Transnational Access Project 'HyperStress'). The work of D. S. Intrigliolo was supported by the Spanish Ministry of Economy and Competitiveness program "Ramón y Cajal."

S. Delalieux is with the Flemish Institute for Technological Research (VITO), Teledetection and Earth Observation Processes, 2400 Mol, Belgium (e-mail: Stephanie.Delalieux@vito.be).

P. J. Zarco-Tejada is with the MARS-GeoCAP, Institute for Environment and Sustainability (IES), Joint Research Centre (JRC), European Commission, Ispra, Italy, on leave from the Instituto de Agricultura Sostenible (IAS), Consejo Superior de Investigaciones Científicas (CSIC), 14004 Córdoba, Spain (e-mail: pzarco@ias.csic.es).

L. Tits is with the Department of Biosystems, KU Leuven, 3001 Heverlee, Belgium (e-mail: Laurent.Tits@biw.kuleuven.be).

M. Á. J. Bello is with the Polytechnic University of Valencia, 46022 Valencia, Spain (e-mail: jimenez_mig@gva.es).

D. S. Intrigliolo is with the Valencia Institute of Agricultural Research (IVIA), 46022 Valencia, Spain.

B. Somers is with the Division of Forest, Nature, and Landscape of the KU Leuven, 3001 Heverlee, Belgium (ben.somers@ees.kuleuven.be).

Color versions of one or more of the figures in this paper are available online at http://ieeexplore.ieee.org.

Digital Object Identifier 10.1109/JSTARS.2014.2330352

I. Introduction

FOR many precision farming applications, the continuous retrieval of spatial, spectral, and/or thermal variability within heterogeneous crops is of great importance. This detailed information is needed for identifying vegetation stress, which is one of the major factors influencing farming management decisions making. Since wilting and dying of plants only occur at extreme developed stress stages, a visual inspection of vegetation health status is most often not time-efficient to avoid yield losses.

Numerous studies have focused on early, nondestructive stress detection for more efficient crop management practices. From these, we can conclude that the physiological responses to stress can be captured in reflectance signals and temperature profiles [1]–[3]. Methods regarding canopy temperature were mainly focused on the effects of water stress on stomatal closure and thermal energy dissipation pathways. In 1982, Idso [4] found out that a large difference between canopy temperature and ambient temperature (Tc–Ta) was associated with water stressed plants, whereas low difference values were associated with well-irrigated plots. Other studies mainly focused on reflectance patterns. Vegetation indices (VIs) provide a very simple yet elegant method for extracting the green plant quantity signal from complex canopy spectra. Often computed as differences, ratios, or linear combinations of reflected light in visible and NIR wavebands [5]–[8], VIs exploit the basic differences between soil and plant spectra. Broad waveband Vis, however, typically lacks diagnostic capability for identifying a particular type of stress or for determining why biomass is at a certain level. Narrower band, hyperspectral, indices such as the Photochemical Reflectance Index (PRI), Water Band Index (WBI), and Normalized Pigment Chlorophyll Ratio Index (NPCI) are examples of reflectance indices that are correlated with certain physiological plant responses and have promise for diagnosing water and nutrient stress [9]–[11].

Next to the high spectral and temporal resolution imagery needed to timely capture subtle differences in reflectance spectra caused by plant physiological responses, also high spatial

resolution data are needed. Suarez *et al.* [12], e.g., indicated the importance of acquiring very high spatial resolution imagery (~ 0.2 m) for assessing fruit quality and water stress in citrus and olive orchards. Stuckens *et al.* [13] came to a similar conclusion when exploring the number of spectrally mixed pixels (i.e., trees, weeds and/or soil all occur within a single image pixel) in simulated orchards. They concluded that pixel sizes should be smaller than 1 m in order to obtain a minimum of 50% pure pixels and smaller than 10 cm for 82% pure pixels. Followup studies demonstrated that these mixing effects of plants and background/litter, whether linear or nonlinear, play an important role in obstructing a detailed assessment of crop conditions in these heterogeneous architectures [14], [15].

Until recently, it was not feasible or affordable to capture high spectral, spatial, and temporal resolution image datasets. For high temporal resolution imagery, one should refer to spaceborne data. However, due to physical limitations and data-transfer requirements the design and development of spaceborne remote sensors face a tradeoff between the spatial and spectral resolution [16]. The Hyperion sensor on board the EO-1 satellite currently offers the highest spectral resolution available from space. The spatial resolution of 30 m restricts, however, a proper use of the inherent potential of these data for detailed mapping purposes [17] and precision farming applications [18]. On the other hand, sensors such as Quickbird and WorldView-2 are able to offer very high spatial resolution imagery, but at the expense of their spectral resolution: panchromatic at submeter spatial resolution, and 4 (Quickbird) to 8 (Worldview-2) broad spectral bands with approximately 2.5 m spatial resolution. With the launch of new high-resolution (HR) satellites such as Worldview-3 and planned hyperspectral missions like Enmap [19], [20], Prisma [21], and Hyspiri [22] much more data will become available to the user community. Still, the tradeoff in spectral and spatial resolution will remain and new advanced data and decision fusion approaches are needed to make optimal use of the future sensor ensembles.

Full-range (400–2500 nm) hyperspectral airborne sensors such as Airborne Prism EXperiment (APEX), Airborne Hyperspectral Scanner (AHS), Airborne Visible/Infrared Imaging Spectrometer (AVIRIS), and Hyperspectral Mapper (Hymap), also face this spectral–spatial resolution tradeoff [16]. These hyperspectral airborne sensors are limited to a spatial resolution of around 2 m, which for the above mentioned precision farming application might not be sufficient. Novel hyperspectral sensors, such as HYSPEX and FIRST, could be mounted on a manned aircraft which, when flying very low, might provide high spatial and spectral resolution data. However, due to the high operational cost of manned flight campaigns, the temporal resolution of this kind of data will be limited.

Innovative developments in Remotely Piloted Aircraft Systems (RPAS) platforms and associated sensing technologies are nowadays expanding at an increasing rate, bringing image resolutions to unprecedented levels of detail, thereby opening exciting new application opportunities [23]. This is especially of huge interest to the precision farming community [24], which requires flexible and frequent data capturing. Although, mainly due to payload restrictions, full-range optical hyperspectral sensors (i.e., ranging from 350 to 2500 nm) are not yet suited to be operated in an operational manner on these lightweight RPAS platforms proposed for precision agriculture. Only few studies have successfully tested pushbroom hyperspectral VNIR sensors on a small, lightweight, fixed-wing RPAS [25].

In an attempt to overcome current spatial, spectral, temporal resolution tradeoffs in spectral sensor design, this study investigates the possibility of assembling a promising new data source through fusing very-high spatial and high spectral imagery based on unmixing techniques, as such enabling more detailed monitoring purposes. We thereby hypothesize that the combination of the high spatial resolution imagery captured by a sensor mounted on a RPAS and the more detailed spectral information available from airborne hyperspectral sensors, albeit at lower spatial resolution, can help to overcome the spatial–spectral data availability tradeoff. Reviews of data fusion methods can be found in [26] and [27]. An interesting unmixing-based fusion technique was previously proposed by Zurita-Milla *et al.* [28], who extended on the work of Zhukov *et al.* [29] and Filiberti [30]. In each of these studies, a multisensor, multiresolution fusion technique was applied to unmix low spatial resolution images using the information about their pixel composition from coregistered high spatial resolution images. Yet, none of these studies were performed on very high spatial (cm resolution) and hyperspectral datasets. Filiberti [30] merged a high-spatial-resolution panchromatic band with a low-spatial-resolution multispectral Landsat TM band with a 1:2 ground sample distance (GSD) ratio between the panchromatic (15 m) and the TM multispectral band (30 m). As such, he aimed at restoring the multispectral image using content from the higher resolution panchromatic image. Zurita-Milla *et al.* [28] showed that the unmixing-based data fusion approach can be used to successfully downscale MERIS FR information (300 m pixel size, 15 bands) to a Landsat-like spatial resolution (25 m pixel size, 6 bands) and as such obtain better MERIS land products. They successfully used the MERIS fused images to assess vegetation status by evaluating the Normalized Difference Vegetation Index (NDVI), the Modified Transformed Chlorophyll Index (MTCI), and the Modified Green Vegetation Index (MGVI).

To address the needs for the early detection of vegetation stress, i.e., high detailed, hyperspectral, and frequent data, we investigated the added value of unmixing-based fusion of unmanned aerial systems and airborne hyperspectral imagery. A spatial unmixing fusion algorithm is, therefore, implemented and applied on simulated and experimental hyperspatial and hyperspectral citrus orchard image datasets. The simulated citrus orchard thereby serves as a preliminary validation tool for the fusion algorithm. For the *in situ* datasets, the fusion process is applied on the most detailed information available both spectrally and spatially. Hyperspatial (cm) images are gathered by a thermal sensor installed on a highly flexible RPAS, whereas the hyperspectral data are acquired by the APEX sensor. The hyperspectral and hyperspatial datasets are fused or spatially unmixed (SpU) in order to assess the performance of narrowband physiological indices for estimating water stress levels in citrus orchards at a 20-cm scale.

II. Methods

A. Drought Stress Assessment

Stem water potential (ψ_stem) is known to be a reliable plant-based water status indicator for irrigation scheduling in fruit trees [31], [32]. However, its measurement is a cumbersome procedure and requires frequent trips to the field and a significant input of labor. Measurements of the stem water potential are, therefore, not useful to monitor drought stress in an operational way.

For that reason, spectral VIs were preferred for estimating water stress from complex canopy spectra, since they provide a simple and efficient method to do so. The NDVI is probably the most studied and implemented vegetation index ever [33]. The NDVI makes use of the characteristic features of vegetative reflectance spectra, namely low reflectance in the red region of the spectrum due to chlorophyll absorption and high reflectance values in the near infrared domain due to scattering caused by internal leaf structure. The optimal information on the physiological status of a plant is, however, not necessarily related to those two regions. Moreover, the NDVI is often not a good indicator of stress as it is only accurate for Leaf Area Index (LAI) (defined as the one-sided green leaf area per unit ground surface area), biomass, and chlorophyll determination at relatively low factor levels, due to a saturation effect at higher levels of those factors [34], [35]. The theory that underpins this vegetation index is, however, promising. Standardized indices have the potential of estimating biophysical parameters in a manner more meaningful than simple ratio indices due to their inherent characteristic of reducing the effects of spectral variations caused by surface topography [36] and sun elevation for different parts of an image. In line with this assumption, the standardized difference of the simulated spectral reflectance values [of low-resolution hyperspectral (LR-HS), HR, high-resolution hyperspectral (HR-HS) images], and of the unmixing-based fused HR, hyperspectral image, referred to as SpU image was calculated for each possible combination of two different wavelengths for realistic ranges of chlorophyll and water content values (1) [37]

$$SDVI = \frac{\lambda_i - \lambda_j}{\lambda_i + \lambda_j} \tag{1}$$

with λ_i and λ_j being the spectral reflectance at wavelength i and wavelength j, respectively, with i and j ranging from 400 to 2500 nm.

Since the data in the validation experiment was simulated, the portions or fractions of soil and vegetation for each pixel were known as well. Multiplying these fractions with the leaf water and chlorophyll content values enabled the reconstruction of reference water and chlorophyll maps. Hitherto, two reference biophysical parameter maps and four spectral images (LR-HS, HR, HR-HS, and SpU) were available. A map representing the coefficients of determination (R^2) of the linear relationship between each possible SDVI map and the reference water and chlorophyll maps was then calculated. This approach allowed the selection of an optimal SDVI to estimate water and chlorophyll content and in the meantime allowed to check how well the commonly used biophysical parameter related VIs perform on the 1) hyperspectral-low spatial (LR-HS), 2) hyperspatial–hyperspectral (HR-HS), and the 3) fused hyperspectral–hyperspatial (SpU) dataset.

TABLE I
Coefficients of Determination R^2 Obtained Through Narrowband Indices From APEX and SpU Imagery Against Stem Potential

VI	SpU−ψ	APEX−ψ
PRI570	0.62 ***	0.21
BRI2	0.47 **	0.29*
R_{515}/R_{570}	0.42 *	0.16
R_{515}/R_{670}	0.38 *	0.14
ZM	0.35 *	0.12
OSAVI	0.34 *	0.05
G	0.34 *	0.14
NDVI	0.34 *	0.13
SR	0.34 *	0.13
MSR	0.34 *	0.12
VOG1	0.31 *	0.09
PRI515	0.24	0.09
R_{520}/R_{500}	0.23	0.05
TCARI	0.14	0.02
RDVI	0.13	0.02

*$p < 0.05$,
**$p < 0.01$,
***$p < 0.001$.

Since narrowband indices (Table I) closely related to the 1) epoxidation state of the xanthophylls cycle; 2) chlorophyll $\mathrm{a} + \mathrm{b}$ concentration; 3) blue/green/red ratio indices; 4) carotenoid concentration; and 5) tree crown structure have been applied in a previous study to detect water stress in citrus orchards at the tree level [11], our focus was reoriented on these indices for the experimental study. Zarco-Tejada concluded from his study that the xanthophyll pigment related PRI calculated with the 570 nm (PRI570) [38] as well as with 515 nm (PRI515) band as a reference [39], was significantly related to the stem water potential, and as such indirectly to the water status of the plant. Also in other studies, PRI has been used to assess previsual water stress at leaf level [40], [41], at canopy level [42]–[44] and using airborne imaging spectroscopy [45]. The PRI index [38], [46] is based on the short-term reversible xanthophyll pigment changes accompanying plant stress [9], [47]. These changes are linked to the dissipation of excess absorbed energy that cannot be processed through photosynthesis [10], [48]–[51]. At the leaf and canopy levels, the PRI has been extensively found adequate to estimate photosynthetic performance [52].

Also the Transformed Chlorophyll Absorption Ratio Index (TCARI) showed sensitivity to stress levels, and the blue/green ratio BGI1 was highly significant. The effects of water stress on the canopy structure were successfully captured by structural indices such as NDVI, RDVI, SR, MSR, OSAVI, TVI, and MTVI. For the 14 trees under investigation in the three selected orchards of the study area, the correlation between all possible SDVIs, including the above-mentioned indices, and the stem water potential was calculated. The index pixel values of the fused image (28 cm) were averaged over each tree. A linear relationship was sought between the VIs, calculated from the fused and the original APEX datasets, and the *in situ* measured stem water potentials as well as between the thermal data and the stem water potentials.

B. Fusion Method—SpU

SpU is a fusion technique, which aims at combining the detailed information from two images over the same study area: one with low spatial and high spectral resolution (in our case a hyperspectral airborne image), and one with high spatial and low spectral resolution (in our case a thermal RPAS image) [28], [29].

In order to easily understand this fusion method, some theoretical background knowledge on spectral unmixing or spectral mixture analysis (SMA) is required. Therefore, we hereby shortly introduce this commonly used image analysis technique, which converts mixed pixel reflectance values into numerical subpixel fractions of a few ground components [53]. Although nonlinear mixing effects are well-acknowledged in vegetated areas [54], [55], [14], [96], [97], linear mixing models have proven to be adequate in the monitoring of vegetative systems [59], [60]. In the linear mixing model, mixed pixel signals (r) are modeled as a linear combination of pure spectral signatures of its constituent components (i.e., endmembers), weighted by their subpixel fractional cover [56]

$$r = Mf + \varepsilon. \tag{2}$$

In (2), M is a matrix in which each column corresponds to the spectral signal of a specific endmember. f is a column vector $[f1, \ldots, fm]^T$ denoting the cover fractions occupied by each of the m endmembers in the pixel. ε is the portion of the spectrum that cannot be modeled using these endmembers. A critical success factor of SMA is the selection of appropriate endmembers [57], [58]. The spectral signatures of the endmembers may be 1) derived from spectral libraries built from field or laboratory measurements, obtained using ground-based or portable spectroradiometers (e.g., [59], [60]); 2) derived directly from the image data themselves (e.g., [61]–[63]); or 3) simulated using radiative transfer models (e.g., [64]–[66], Once the endmembers and their spectral signatures are known and if the number of endmembers is less than the number of spectral bands, the system of (1) is over-determined and may uniquely be inverted using techniques to solve for the fractions to solve for the fractions minimizing the error term ε in (2). Least squares regression analysis is one of the most commonly used optimization techniques [67]. SMA can be implemented without constraints (e.g., [68]), but physically meaningful abundance estimates are often obtained by constraining the coefficients in (2) to sum to unity and to be positive [69], [70].

The SpU fusion algorithm applied in this study differs from spectral unmixing as it tries to recover the spectra for endmember classes within a pixel, instead of the cover fractions of the different materials. The material fractions can be deduced from the high spatial, low spectral resolution RPAS image. Fig. 1 gives a visual representation of the spatial unmixing technique. Several steps are involved in the procedure starting with the classification of the high spatial resolution image in m classes (*in casu*, soil, and vegetation). Fraction maps F are subsequently created per predefined kernel k (*in casu*, five by five) of the hyperspectral pixels, by counting for each class the amount of HR pixels, which are present in the corresponding lower resolution pixel. Once the fraction maps F are calculated and given the hyperspectral reflectance values for the hyperspectral pixels R at a particular

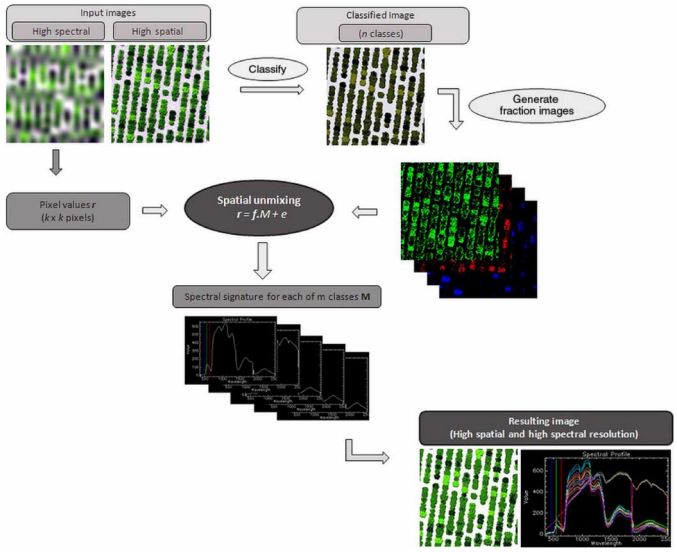

Fig. 1. Overview of the spatial unmixing technique.

wavelength of interest, the spatial unmixing equation can be solved by least squares optimization, in order to find the reflectance value at that particular wavelength of the class endmembers M. The unmixing is thus solved for each low spatial resolution band independently. Therefore, a kernel size larger than or equal to the number of classes present in the neighborhood had to be chosen, because each hyperspectral pixel provides only one mixing equation [28]. Finally, each of the m classes present in the central pixel of the kernel is replaced by its corresponding unmixed signal. By repeating this operation for all the airborne hyperspectral pixels and bands, and for different combinations of m and k, a series of fused images is generated in which endmember variability is induced, which can be seen as a major benefit of this unmixing-based fusion method [69].

Analogous to (2), the unmixing-based fusion method can be defined as follows:

$$R^{i,k} = M^{i,k,m} \cdot F^{k,m} + \varepsilon. \tag{3}$$

In (3), $R^{i,k}$ is a vector that contains the values of band i for all the hyperspectral pixels present in the neighborhood k. $M^{i,k,m}$ is the unknown vector containing spectral information of each of the classes present in k. $F^{k,m}$ is a matrix containing the cover fractions occupied by each of the m endmembers in each pixel in k. ε is the portion of the spectrum that cannot be modeled.

This indirectly implies that the number of classes (m) and the size of the neighborhood (k) need to be optimized. m needs to be optimized based on the application demand and on the spectral variability of the scene. k also needs to be optimized because it has a great impact on the spectral quality of the fused image.

The performance of the fusion method was first tested on a simulated dataset, which is further described in detail in Section III-A.

A robust classification of the hyperspatial image was achieved by the linear discriminant analysis method with endmember selection as available in the open source ENVI/IDL code [71]. After a sensitivity analysis (results not shown), a kernel size of 5×5 pixels was defined as optimal for spatial unmixing of these

datasets. Changing the kernel size had a major impact on the endmember variability in the scene and played an important role in the reconstruction of the hyperspectral signatures.

Next to the assessment of the index performances, the hyperspectral signatures reconstruction through unmixing-based fusion was evaluated as well. The root-mean-square error (RMSE) and relative-root-mean-square error (RRMSE) were calculated to compare the hyperspectral signals from the reference HR-HS image and the modeled signals from the SpU and LR-HS (upscaling with a factor 10) images. RMSE, defined (4), is a measure of the standard deviation, whereas RRMSE, defined in (5), is RMSE as a percentage of the mean observation. RMSE and RRMSE should be as small as possible, optimally zero

$$RMSE = \sqrt{\sum_{i=1}^{n} \frac{(O_i - P_i)^2}{n}} \tag{4}$$

$$RRMSE = \sqrt{\sum_{i=1}^{n} \frac{(O_i - P_i)^2}{n}} \cdot \frac{1}{\overline{O}}. \tag{5}$$

In (4) and (5), O_i is the reference or observed value at wavelength i; P_i the predicted value at wavelength i; n the total amount of measurements; and $\overline{O}$ the average of the observations.

After validating the fusion algorithm on a simulated dataset, the algorithm was applied on an experimental dataset, which is described in Section III-B. By fusing the information from the hyperspectral (APEX) and hyperspatial (thermal RPAS) datasets into an SpU, hyperspatial, hyperspectral resolution scene (SpU), we aimed at a more efficient assessment of the level of water stress in capital intensive citrus orchards. The thermal RPAS data were, therefore, classified in three physiological meaningful temperature classes. A kernel size of 5×5 was defined as most optimal. Combining different kinds of images requires a perfect coregistration. Fifteen ground control points (GCPs) were identified in both images for this purpose.

III. Materials

A. Simulated Data Experiment

For this study, a ray-tracing experiment in a fully calibrated virtual 3-D representation of a citrus orchard was used. This 3-D radiative transfer model has been integrated in the web-based RAMI Online Model Checker (ROMC) service [72], and has previously been used as a reference tool for validation of image analysis techniques for precision farming (e.g., [18], [66], Based on detailed *in situ* calibration measurements, virtual 3-D replicas of orchard trees were built as triangular meshes using a tree geometry algorithm developed in Weber and Penn [73] (Fig. 2).

All reference data for calibration (and validation) were collected in a 9-year-old Valencia "Midknight" orange grove near Wellington, South Africa (33°13′60″S; 18°15′60″E, altitude 100 m). The orchard block had a row spacing of 4.5 m, a tree spacing of 2 m, and a row azimuth of 7.3°. For each tree, dendrometric (LAI, height, crown width, and diameter) and optical properties (leaf and canopy reflectance) were determined. Canopy and leaf reflectance spectra were collected using an ASD

Fig. 2. (Left) a virtual 3-D replica of an orchard tree, (right) a real orchard tree.

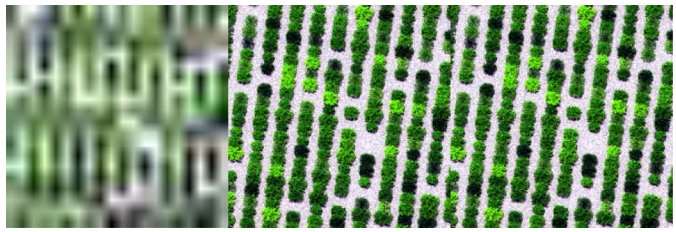

Fig. 3. RGB representation of the synthetic images of the virtual orchard (left: LR-HS—2 m, center: HR—0.2 m and right: HR-HS—0.2 m) generated using a modified version of a physically based ray-tracer.

FR spectroradiometer (Analytical Spectral Devices, Boulder, CO) ranging from 350 to 2500 nm with a spectral resolution of 3 nm in the VIS and NIR and 10 nm in the SWIR. The noise level for this instrument is provided by the manufacturer as $1.0\times10^{-9}\mathrm{W/cm^2/nm/sr}$ at 700 nm, $1.4\times10^{-9}\mathrm{W/cm^2/nm/sr}$ at 1400 nm, and $2.2\times10^{-9}\mathrm{W/cm^2/nm/sr}$ at 2100 nm. A 25° field of view (FOV) bare fiber optic was used. Within the orchard, 60 trees were selected that cover the range of structural and spectral variability encountered in the orchard. Leaf chlorophyll and water content were derived from the measured leaf spectra through inversion of the PROSPECT model [74]. These field measurements were used to calibrate 3-D replicas of the measured trees. In order to increase the observed variability in tree conditions, we further created for each of the 3-D trees three additional clones. While the overall tree architecture remained the same, we created 1) one clone with similar leaf spectra but with a LAI, which was 56% of the reference trees by randomly removing part of the leaves; 2) one clone with similar LAI and leaf water content but reduced leaf chlorophyll content (50% of the reference chlorophyll) (note that the new reflectance coefficients were recalculated with the PROSPECT model [75]); and 3) one clone with similar LAI and leaf chlorophyll but reduced water content (70% of reference). The new reflectance coefficients were recalculated with the PROSPECT model [75]. Thus, extra variability in the biophysical parameters and the spectral data were created to incorporate different types of stress. All 3-D tree replicas were then randomly placed in the orchard. The physical and optical properties of the soil (sandy texture, gravimetric moisture content ranging between 0% and 15%) were determined in the field and applied in the virtual model. Full details on the calibration procedure can be found in Stuckens *et al.* [75], whereas a more detailed description of the field campaign can be found in Somers *et al.* [76].

Three synthetic images of the virtual orchard were generated using a modified version of a physically based ray-tracer [77] (Fig. 3, The first image of 400×400 pixels provided information in 216 spectral bands ranging from 350 to 2500 nm with a

spectral resolution of 10 nm and a spatial resolution of 2 m (referred to as, low-resolution–hyperspectral or LR-HS, left panel of Fig. 3). This is comparable to the resolutions obtained by airborne hyperspectral sensors, such as APEX and CASI.

The second scene, depicted in the center panel of Fig. 3, represents an image captured by a RGB sensor onboard a RPAS. The image of 4000×4000 pixels with a spatial resolution of 0.2 m is further referred to as high resolution or HR) (Fig. 3, center panel). The third or reference image scene simulated a 216-band hyperspectral sensor ranging from 350 to 2500 nm with a spectral resolution of 10 nm and a spatial resolution of 0.20 m (high resolution-hyperspectral or HR-HS). Such detailed imagery is currently not yet achievable on a recurrent basis (high temporal resolution) by satellite or airborne systems. The airborne hyperspectral cameras, such as Hyspex, can possibly be used in manned aircrafts to gather high spatial and spectral resolution data, but the temporal resolution will be limited due to financial constraints (manned aircrafts are expensive). Notwithstanding this, it serves as a perfect reference scene to test the efficiency of the unmixing-based data fusion of the first two image scenes.

For each simulated image scene, detailed fraction maps (cf. Section II-B) were available.

B. Real Data Experiment

An additional experiment was conducted in a 310-ha drip irrigated commercial Citrus orchard near Picassent, in the province of Valencia (Spain, 39.38N, 0.475E, altitude 47 m). In Citrus, an accurate and previsual detection of water stress is of utmost economic importance for farmers [78]. The orchard design was characterized by large (5–6 m) row spacing, with canopy ground cover below 65% even in the more vigorous orchards. Three test orchards were selected based on the large variation in plant water status of the measured trees. A total of 14 trees were used for assessment of midday stem water potential (ψ_s) determined using a pressure chamber in leaves that were bagged at least 1 h prior to the measurements. Stem water potential was chosen as the true field determination of citrus trees water status due to its sensitivity to water deprivation [79]. The ψ_s measurements of each tree were related with the individual tree canopy temperature (Tc) extracted from the airborne imagery. Within the selected trees, ψ_s varied from -0.6 to -2.0 MPa. According to a previous study by Ballester *et al.* [80], these values correspond to well watered and relatively severe tree water stress conditions, respectively.

Airborne hyperspectral APEX imagery was acquired over the study area on September 8, 2011 around solar noon. The air temperature and vapor pressure deficit (VPD) at the time of the flight were 30.4° and 2.1 kPa, respectively. The APEX sensor recorded the reflected light in 288 bands, ranging from 380 to 2500 nm with a spatial resolution of 2.7 m. The airborne measurements were accompanied with spectral field and lab measurements for calibration and validation of the airborne data. APEX geometric correction was accomplished based on the delivered metadata (i.e., IMU). Atmospheric correction was performed with the processing chain of VITO, based on the algorithms of ATCOR [81]. The geometric correction was performed by VITO's own developed C++ module and is based on direct georeferencing. Input data from the sensor's GPS/IMU, boresight correction data and the SRTM DEM were further used during the geometric correction process (Fig. 4).

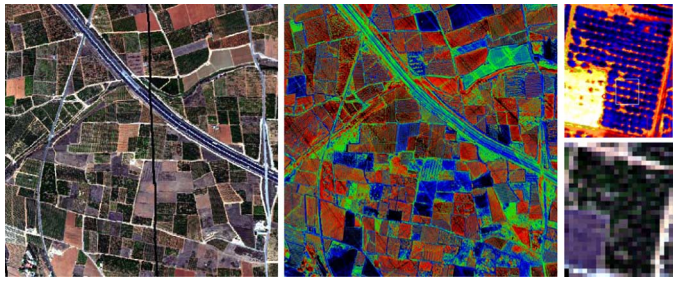

Fig. 4. Left: APEX region of interest with 288 spectral bands and 2.80 m spatial resolution, mid: RPAS region of interest with 1 thermal band and 0.28 m spatial resolution. Right top: $10\times$ zoom of APEX orchard with 288 spectral bands and 2.80 m spatial resolution, right bottom: RPAS orchard with 1 thermal band and 0.28 m spatial resolution.

Another set of aerial images was collected on August 23, 2011 at 10:00 GMT time with a thermal sensor installed on a RPAS, acquiring imagery at 20 cm resolution. A thermal camera (Miricle 307 K; Thermoteknix Systems Ltd, Cambridge, U.K.) was installed on a RPAS developed at the Laboratory for Research Methods in Quantitative Remote Sensing (Quantalab; IAS-CSIC, Córdoba, Spain), as described by Zarco-Tejada *et al.* [25]. The camera has a resolution of 640×480 pixels, is equipped with a 14.25-mm f1.3 lens, and is connected to a computer via a USB 2.0 protocol. The spectral response was in the range $8 - 12$ μm.

The air temperature and VPD at the time of the flight were 31.6° and 1.9 kPa, respectively. The camera was calibrated in the laboratory to obtain radiance values, and then upwelling and down welling sky temperature was measured during the flight. In addition, indirect calibrations were conducted using surface temperature measurements to improve the calibration. The accuracy of this method was evaluated by Berni *et al.* [23], who have demonstrated an accuracy less than 1 K. The mosaicking process selects only the most nadir part of the overlapping images, limiting the viewing angle and thus avoiding directional effects and thermal hotspot. Each snapshot had a relative temperature scale, being the minimum value the coldest pixel and the maximum value the hottest pixel of the snapshot [23].

Based on the temperature differences between plant canopy and air temperature (Tc-Ta), all background and nonphotosynthetic trees were masked. This region of interest was subsequently overlaid on the APEX image to remove all redundant information from the APEX scene. This, however, also implied the removal of all warm, i.e., nontranspiring and/or dead trees.

The hyperspectral APEX and hyperspatial, thermal images were resampled to 2.8 and 0.28 m, respectively.

IV. Results and Discussion

A. Simulated Dataset

The unmixing-based fusion of the LR-HS and HR simulated image data resulted in an SpU image containing 216 bands at 20 cm resolution. The fused image product (SpU) now contains

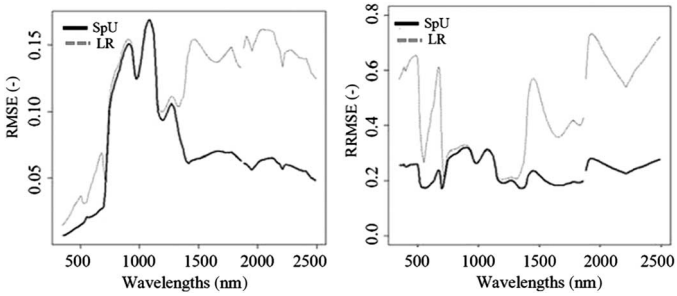

Fig. 5. RMSE (left) and RRMSE (right) plots calculated from the reference spectra and 1) the reconstructed SpU spectra and 2) the downscaled LR-HS spectra.

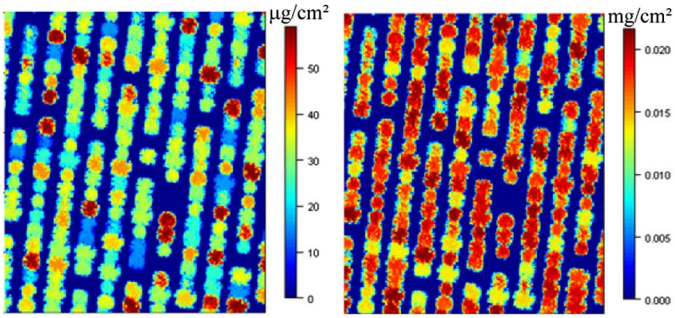

Fig. 6. The reference chlorophyll (left) and water map (right).

more detailed spectral and spatial information on the individual image elements or endmembers (e.g., orchard trees). This becomes clearer when looking into the results of the hyperspectral signature reconstruction evaluation study (Fig. 5).

Overall, we observed a significant increase in signature modeling accuracy compared to the spectra of the LR image. The increased accuracy was specifically remarkable in the 350–800 nm and 1200–2500 nm domain, which is most probably due to the higher differences between soil and vegetation spectra in these spectral regions [76]. This highlights that the spectral mixing of vegetation and soil spectra, which remains the main bottleneck when using LR imagery in precision agriculture [13], [82], [18], can, to a large extent, be solved by SpU.

By better modeling the spatial variability in crop spectra—i.e., by removing the effects of undesired background effects—SpU opens new opportunities for the site-specific monitoring of the condition of crops (i.e., precision farming). In this light, we evaluated the added value of the proposed method in estimating the crop canopy water and chlorophyll content. Recall that for this simulated scene we reconstructed HR (0.2 m resolution) reference maps of the chlorophyll ($\mathrm{Chl_{ref}}$) and water ($\mathrm{C_{w\ REF}}$) content of the crop canopies (Fig. 6). For each simulated image, i.e., HR, LR-HS, and HR-HS, the coefficients of determination ($\mathrm{R^2}$) of the linear regression between all possible SDVIs and the water ($\mathrm{C_{w\,REF}}$) and chlorophyll ($\mathrm{Chl_{ref}}$) content maps are summarized in Fig. 7.

As expected, the SDVI's most closely related to chlorophyll and water content, were mainly identical throughout the three images. For the LR-HS ($\mathrm{spatial\ resolution} = 2\ \mathrm{m}$) image a maximum $\mathrm{R^2}$ of 0.35 and 0.30 were observed for water and chlorophyll, respectively. A significant increase in predictive power was found for the SpU image with maximal $\mathrm{R^2}$ values up to 0.77 for water and 0.71 for chlorophyll. The most appropriate water and chlorophyll related indices contain wavebands corresponding to the highest coefficient of absorption by water (SWIR) [83] and chlorophyll (620–700 nm) [84], respectively. It has to be mentioned that these spectral regions correspond to the regions with the highest gain in signature modeling accuracy by applying the unmixing-based fusion compared to the original LR-HS and HR images (Fig. 5). This noticeably stresses the potential of the proposed technique for better estimating plant stress related to changes in biochemical parameter contents, such as chlorophyll and water.

From Fig. 7, it was revealed that the best SDVIs to estimate canopy water (6) and chlorophyll content (7) were, respectively

$$\frac{\lambda_{730} - \lambda_{1510}}{\lambda_{730} + \lambda_{1510}} \tag{6}$$

$$\frac{\lambda_{540} - \lambda_{590}}{\lambda_{540} + \lambda_{590}}. \tag{7}$$

The corresponding SDVI maps are shown in Figs. 8 and 9. For easy interpretation, and to allow a fair comparison, also the reference water ($\mathrm{C_{w\,REF}}$) and chlorophyll ($\mathrm{Chl_{ref}}$) maps are shown.

Coefficients of determination ($\mathrm{R^2}$) calculated for the linear regression between the reference ($\mathrm{C_{w\,REF}}$ and $\mathrm{Chl_{ref}}$) maps and the most appropriate SDVI (6) and (7) maps, showed significant differences in prediction accuracy for SpU ($\mathrm{C_{w\ SpU}}$: $\mathrm{R^2} = 0.77$ and $\mathrm{Chl_{SpU}}$: $\mathrm{R^2} = 0.71$), compared to the original LR image ($\mathrm{C_{w\ LR}}$: $\mathrm{R^2} = 0.35$ and $\mathrm{Chl_{ref}}$: $\mathrm{R^2} = 0.30$). The highest possible linear relationship between the selected SDVI (6) and (7) maps and the biophysical parameter content maps ($\mathrm{C_{wREF}}$ and $\mathrm{Chl_{ref}}$) is shown in the $\mathrm{C_{w\ HR-HS}}$ (with $\mathrm{R^2} = 0.93$) and the $\mathrm{Chl_{HR-HS}}$ ($\mathrm{R^2} = 0.86$) maps. From these results, we can conclude that the spatial resolution of 2 m can be beneficial for large scale mapping and monitoring of the citrus orchard, e.g., for delineating management zones in the orchard. However, the resolution is too coarse to precisely manage the orchard system in which an optimization of yield with a restricted input of natural resources is endeavored. This corroborated previous findings of Stuckens *et al.* [75] who illustrated that image interpretation in citrus orchards was already seriously aggravated at pixel sizes as small as 0.1 m resolution. At this resolution about 18% of the pixels were still mixed, while for $\mathrm{pixel\ sizes} > 4\ \mathrm{m}$, no pure pixels were present anymore. In addition, Zarco-Tejada *et al.* [85] demonstrated serious effects of soil background admixture on the chlorophyll concentration estimates of olive trees using 1 m ROSIS imagery. The SpU methodology provides a means to combine: 1) the high spatial detail needed to reduce undesired background effects; and 2) the high spectral detail for detailed characterization of the plant state. The data fusion approach as such allows providing adequate information support for agricultural production and accurate and precise management of fruit orchards.

B. Real Data Experiment

Applying the spatial unmixing technique on the 0.28-m thermal RPAS and the 2.8-m hyperspectral APEX datasets

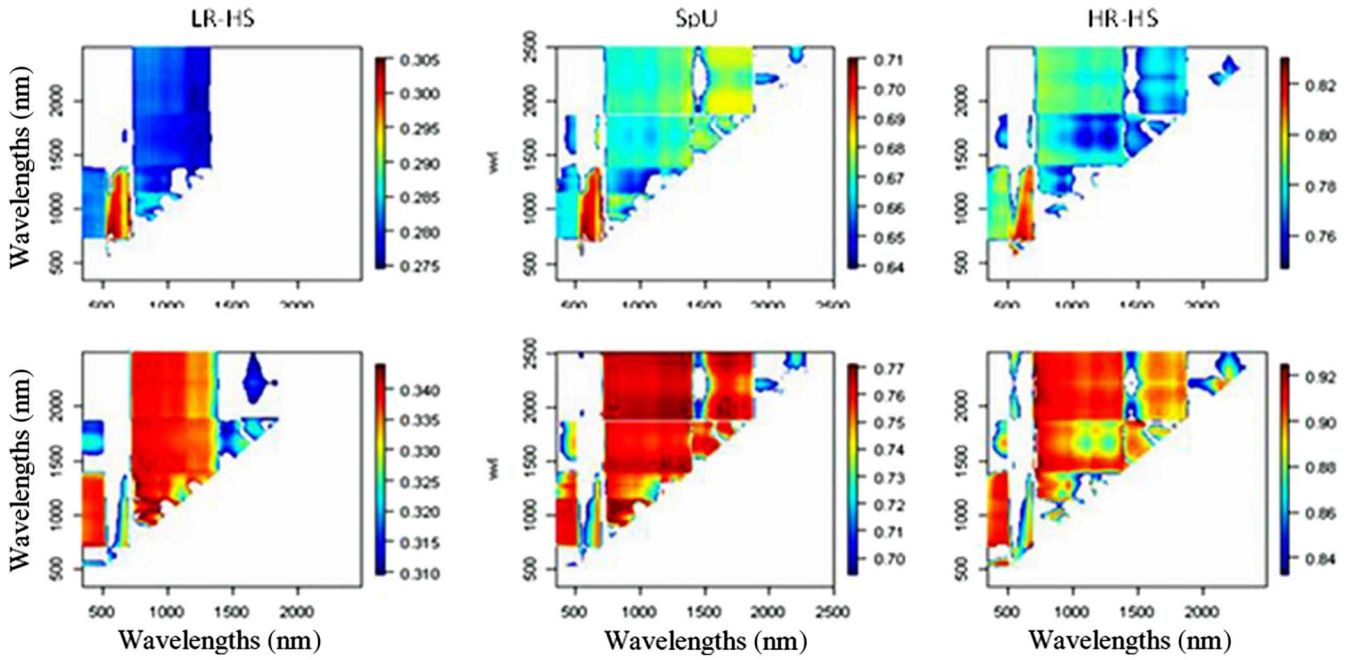

Fig. 7. R^2 values indicating the performances of each possible SDVI to estimate chlorophyll (top) and water content (bottom) of the LR-HS, SpU, and HR-HS simulated images. A lower threshold value is defined for each image to enlarge the color contrast.

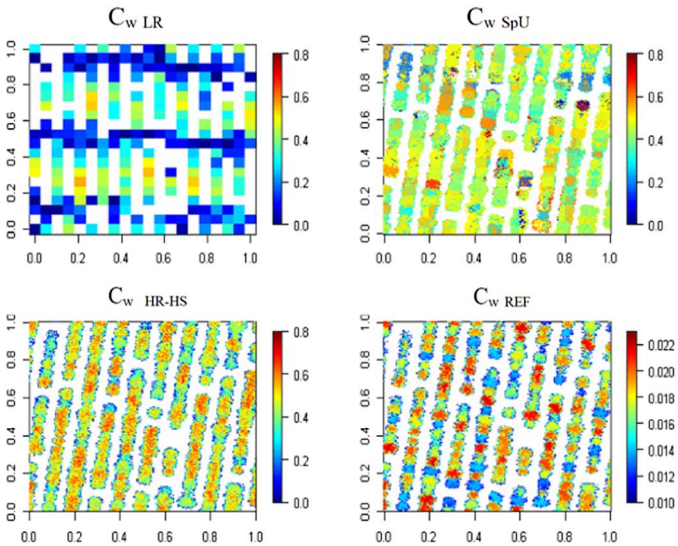

Fig. 8. Index (5) maps representing water content extracted from the LR ($R^2 = 0.34$) (top left), SpU ($R^2 = 0.77$) (top right), HR-HS ($R^2 = 0.93$) (bottom left) images, and reference water content map (bottom right).

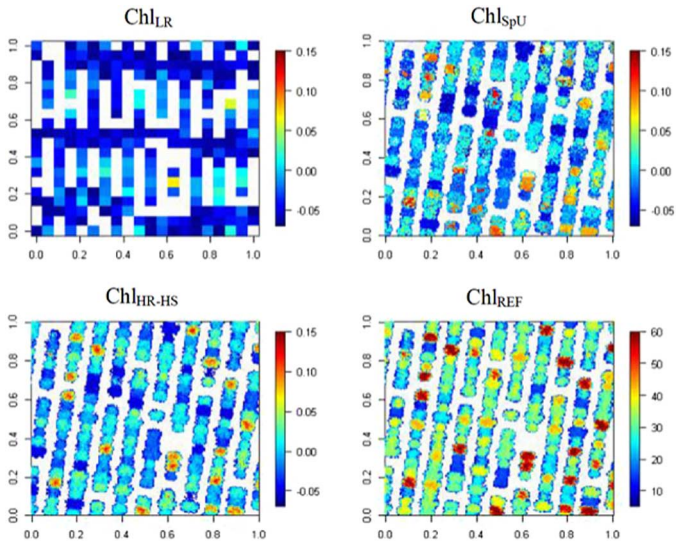

Fig. 9. Index (6) maps representing chlorophyll content extracted from the LR-HS ($R^2 = 0.30$) (top left), SpU ($R^2 = 0.71$) (top right), HR-HS ($R^2 = 0.86$) (bottom left) images, and reference chlorophyll content map (bottom right).

resulted in an SpU image providing 288 bands at 0.28 m spatial resolution (Fig. 10).

A visual inspection of the APEX pixel spectra already revealed an intimate mixture of soils and crops. This could quantitatively be verified, in Table I, comparing the coefficients of determination extracted from the relationship between narrowband index values acquired from the APEX and SpU images, respectively, against the stem water potential values. Results are shown for 21 narrowband stress-related VIs, already previously described in a similar case study in citrus performed by Zarco-Tejada *et al.* [25].

Although similar trends were found for the indexes extracted from the APEX and SpU pixels, an overall better relationship (higher R^2) was found for SpU. Due to the presence or admixture of soil background and vegetation in the larger APEX pixels, all indices performed worse in estimating water stress in the LR-HS APEX image. This was particularly true for the PRI570 index [Table I and Fig. 11, significant relationships ($p < 0.05$) are shown in bold] with $R^2 = 0.62$ for the SpU image compared to $R^2 = 0.21$ for the LR-HS APEX image. The added value of the hyperspatial resolution lies herein that VIs can be applied on pure vegetation pixels without the contribution of soil background and structural effects [15], [18]. Knowing that the stem water potential is a good and reliable estimator of plant water stress, it can be concluded from the relationship shown in Fig. 11 that

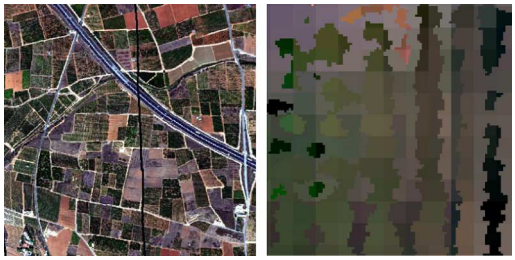

Fig. 10. SpU image and detailed view.

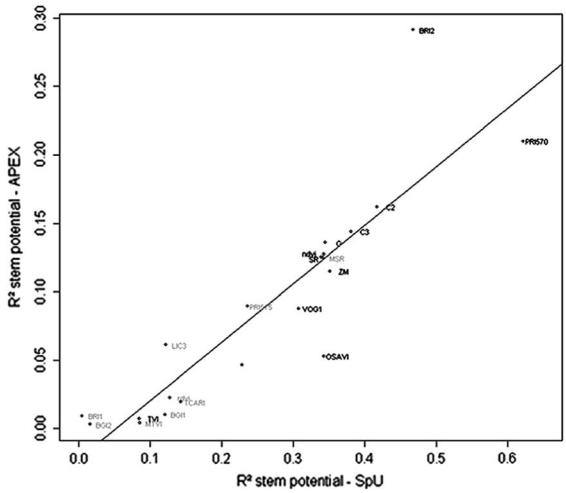

Fig. 11. Representation of the correlation between the coefficients of determination R^2 obtained through narrowband indices from APEX and SpU imagery against stem potential.

detailed spatial information is vital in water stress detection studies.

When we also show results for all other SDVI's in Fig. 12, it becomes clear that an even better water stress detection becomes possible when also the reflectance patterns of the SWIR domain could be captured by the sensor. Numerous previous studies have proven that the spectral behavior of vegetation in the SWIR spectral domain is severely influenced and masked by water absorption. In this study, R^2 values up to 0.81 (compared to 0.62 for PRI570) were obtained through a linear relationship of SpU derived SDVIs based on 562 and 1650 nm against stem water potential. The reflectance absorptions in the 1650–1850-nm region are known to reflect not only the leaf water content, but also the contents of leaf cellulose and lignin, and are directly related to the plant growing status [86], [87].

This is a particularly interesting observation, since current technology does not yet allow to gather such a high spatial, high spectral imagery over the full spectral range with airborne sensors. Yet, by fusing hyperspatial and full range (including SWIR) hyperspectral images we can create a new data source which, as shown in Fig. 12, opens new and promising opportunities for detailed water stress mapping.

From the previous studies [1], [88]–[95], we know that a good correlation should exist between thermal data and water stress or stem potentials, which was not found in our study, due to a miscalibration of the thermal sensor. Within one image, the relationship between stem potentials and thermal data were high

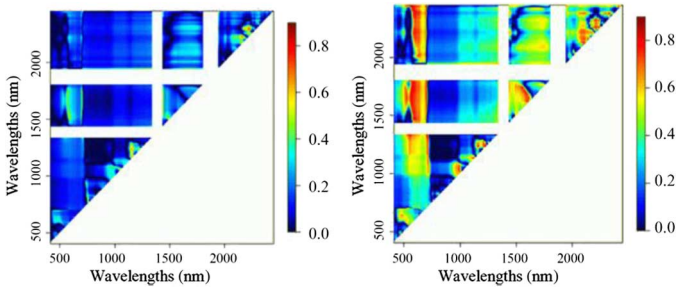

Fig. 12. R^2 values of the linear relationship between the stem water potential of the 14 trees of interest and all possible SDVIs (left) calculated from APEX pixels (right) calculated from SpU pixels. Atmospheric water absorption bands were masked from the analysis.

($R^2 = 0.72$), but not as high as the PRI calculated from the SpU and water potentials relationship ($R^2 = 0.80$) within this same image. The temperature differences caused by the sensor were masked in the fusion method due to its inherent characteristic to reconstruct hyperspectral endmember signatures based on the materials present in the pixels within the kernel.

V. Conclusion

The aim of this study was to apply an unmixing-based fusion technique on a hyperspectral airborne and hyperspatial RPAS dataset for a better assessment of biophysical parameters in agricultural areas. We first tested the unmixing-based fusion method on simulated datasets to evaluate the proposed method through standardized VIs and spectral signature reconstruction. Based on the high correlations between the SDVI performances calculated from the SpU image and those calculated from the reference images, and the high R^2; values of the SDVI biophysical parameter content relations compared to those of the low-resolution (LR) image, we concluded that the SpU method has potential for more detailed research in water and chlorophyll content estimation.

Subsequently, the fusion method was applied on a real test case, in which hyperspectral APEX and hyperspatial thermal RPAS images were combined in order to better and more accurately detect water stress in commercial citrus orchards. Thereby, a better relationship was found between the stem water potential, and the PRI570 index, both known to be good and reliable water stress indicators, when calculated on the fused image compared to the one obtained from the original lower resolution image ($R^2 = 0.62$ vs. 0.21). Furthermore, VIs containing shortwave infrared spectral bands have appeared to make a sound contribution in terms of the strength of relationships between spectral reflectance and water stress levels.

This fusion technique offers new opportunities to the user community in that higher spatial spectral dataset become available for their research or operations. The need for a perfect coregistration of the two input images (i.e., high spatial and high spectral) can be seen as the major drawback of this technique. Efforts have to be made in this processing step, which has a large impact on the resulting fused image if not carefully done. Ideally, the two sensors, of which one is focused on the spatial detail and the other focused on the spectral detail should be mounted on one chip, so that coregistration issues are minimized. This approach

could be extended globally for the fusion of high spatial and high spectral resolution satellite imagery, enabling also a temporal hyperspectral, hyperspatial analysis. Ongoing research focuses on quantification of nonlinear mixing effects in orchards, and its influence on the accuracy of unmixing models. If proven to be important, the implementation of nonlinear mixing models will be necessary to further improve the performance of the proposed algorithm.

Acknowledgment

D. Notario, A. Vera, R. Romero, and A. Hornero are also acknowledged for their technical support during the field and airborne campaigns.

References

[1] R. D. Jackson, S. B. Idso, R. J. Reginato, and W. L. Ehrler, "Crop temperature reveals stress," *Crop Soils*, vol. 29, pp. 10–13, 1977.

[2] S. B. Idso, R. J. Reginato, and R. D. Jackson, "An equation for potential evaporation from soil, water and crop surfaces adaptable to use by remote sensing," *Geophys. Res. Lett.*, vol. 4, pp. 187–188, 1977.

[3] R. D. Jackson and P. J. Pinter, Jr., "Detection of water stress in wheat by measurement of reflected solar and emitted thermal IR radiation," in *Proc. Spectral Signatures Objects Remote Sens. Inst. Nat. de la Recherche Agronom.*, Versailles, France, 1981, pp. 399–406.

[4] S. B. Idso, "Non-water-stressed baselines: A key to measuring and interpreting plant water stress," *Agric. Meteorol.*, vol. 27, pp. 59–70, 1982.

[5] D. W. Deering, J. W. Rouse, Jr., R. H. Haas, and J. S. Schell, "Measuring forage production of grazing units from Landsat MSS data," in *Proc. 10th Int. Symp. Remote Sens. Environ. (ERIM)*, Ann Arbor, Michigan, 1975, pp. 1169–1178.

[6] A. J. Richardson and C. L. Wiegand, "Distinguishing vegetation from soil background information," *Photogr. E. R.*, vol. 43, pp. 1541–1552, 1977.

[7] C. J. Tucker, "Red and photographic infrared linear combinations for monitoring vegetation," *Remote Sens. Environ.*, vol. 8, pp. 127–150, 1979.

[8] R. D. Jackson, "Spectral indices in n-space," *Remote Sens. Environ.*, vol. 13, pp. 409–421, 1983.

[9] J. Peñuelas, J. A. Gamon, A. L. Fredeen, J. Merino, and C. B. Field, "Reflectance indices associated with physiological changes in nitrogen- and water-limited sunflower leaves," *Remote Sens. Environ.*, vol. 48, pp. 135–146, 1994.

[10] J. A. Gamon, L. Serrano, and J. S. Surfus, "The photochemical reflectance index: An optical indicator of photosynthetic radiation use efficiency across species, functional types and nutrient levels," *Oecologia*, vol. 112, pp. 492–501, 1997.

[11] P. J. Zarco-Tejada, V. González-Dugo, and J. A. J. Berni, "Fluorescence, temperature and narrow-band indices acquired from a UAV platform for water stress detection using a micro-hyperspectral imager and a thermal camera," *Remote Sens. Environ.*, vol. 117, pp. 322–337, 2012.

[12] L. Suárez *et al.*, "Detecting water stress effects on fruit quality in orchards with time-series PRI airborne imagery," *Remote Sens. Environ.*, vol. 114, pp. 286–298, 2010.

[13] J. Stuckens *et al.*, "Off-nadir viewing and sensor specifications for reducing spectral mixture issues in Citrus orchards," *Photogramm. Eng. Remote Sens.*, vol. 76, pp. 1261–1274, 2010.

[14] B. Somers, S. Delalieux, W. W. Verstraeten, and P. Coppin, "A conceptual framework for the simultaneous extraction of sub-pixel spatial extent and spectral characteristics of crops," *Photogramm. Eng. Remote Sens.*, vol. 75, pp. 57–68, 2009.

[15] L. Tits, B. Somers, and P. Coppin, "The potential and limitations of a clustering approach for the improved efficiency of multiple endmember spectral mixture analysis in plant production system monitoring," *IEEE Trans. Geosci. Remote Sens.*, vol. 50, no. 6, pp. 2273–2286, Jun. 2012.

[16] M. A. Lefsky, A. Cohen, and B. Warren, "Selection of remotely sensed data," in *Remote Sensing of Forest Environment, Concepts and Case Studies*, M. A. Wulder and S. E. Franklin, Eds. Norwell, MA, USA: Kluwer, 2003, pp. 13–46.

[17] A. Lucieer, S. Robinson, and D. Turner, "Using an unmanned aerial vehicle (UAV) for ultra-high resolution mapping of Antarctic moss beds," in *Proc. 15th Australas. Remote Sens. Photogramm. Conf.*, Alice Springs, Australia, Sep. 14–16, 2010, pp. 429–433.

[18] L. Tits, B. Somers, J. Stuckens, J. Farifteh, and P. Coppin, "Integration of in situ measured soil status and remotely sensed hyperspectral data to improve plant production system monitoring: Concept, perspectives and limitations," *Remote Sens. Environ.*, vol. 128, pp. 197–211, 2013.

[19] T. Stuffler *et al.*, "The EnMAP hyperspectral imager—An advanced optical payload for future applications in Earth observation programmes," *Acta Astronaut.*, vol. 61, no. 1–6, pp. 115–120, Jun./Aug. 2007.

[20] K. Segl *et al.*, "EeteS—The EnMAP end-to-end simulation tool," *IEEE J. Sel. Topics Appl. Earth Observ. Remote Sens.*, vol. 5, no. 2, pp. 522–530, Apr. 2012.

[21] D. Labate *et al.*, "The PRISMA payload optomechanical design, a high performance instrument for a new hyperspectral mission," *Acta Astronaut.*, vol. 65, no. 9–10, pp. 1429–1436, Nov./Dec. 2009.

[22] National Research Council Committee (NRC), *Earth Science and Applications from Space, National Imperatives for the Next Decade and Beyond*. Washington, DC, USA: The National Academies Press, 2007.

[23] J. A. J. Berni, P. J. Zarco-Tejada, L. Suarez, and E. Fereres, "Thermal and narrow-band multispectral remote sensing for vegetation monitoring from an unmanned aerial vehicle," *IEEE Trans. Geosci. Remote Sens.*, vol. 47, no. 3, pp. 722–738, Mar. 2009.

[24] T. Guo, T. Kujirai, and T. Watanabe, "Mapping crop status from an unmanned aerial vehicle for precision agriculture applications," in *Proc. 22nd ISPRS Congr. Int. Arch. Photogramm. Remote Sens. Spat. Inf. Sci.*, Melbourne, Australia, vol. 39-B1, Aug. 25–Sep. 1, 2012, pp. 485–490.

[25] P. J. Zarco-Tejada, V. González-Dugo, and J. A. J. Berni, "Fluorescence, temperature and narrow-band indices acquired from a UAV platform for water stress detection using a micro-hyperspectral imager and a thermal camera," *Remote Sens. Environ.*, vol. 117, pp. 322–337, 2012.

[26] F. Castanedo, "A review of data fusion techniques," *Sci. World J.*, vol. 201, 19p, 2013.

[27] B. Khaleghi, A. Khamis, F. O. Karray, and S. N. Razavi, "Multisensor data fusion: A review of the state-of-the-art," *Inf. Fusion*, vol. 14, pp. 28–44, 2013.

[28] R. Zurita-Milla, J. G. P. W. Clevers, and M. E. Schaepman, "Unmixing-based Landsat TM and MERIS FR data fusion," *IEEE Geosci. Remote Sens. Lett.*, vol. 5, no. 3, pp. 453–457, Jul. 2008.

[29] B. Zhukov, D. Oertel, F. Lanzl, and G. Reinhäckl, "Unmixing-based multisensor multiresolution image fusion," *IEEE Trans. Geosci. Remote Sens.*, vol. 37, no. 3, pp. 1212–1226, May 1999.

[30] D. Filiberti, "Combined spatial-spectral processing of multisource data using thematic content," Ph.D. dissertation, Dept. Elect. Comput. Eng., Univ. Arizona, Tucson, AZ, USA, 2005, 119pp.

[31] K. A. Shackel, H. Ahmadi, and W. Biasi, "Plant water status as an index of irrigation need in deciduous fruit trees," *HortTechnology*, vol. 7, pp. 23–29, 1997.

[32] D. S. Intrigliolo and J. R. Castel, "Usefulness of diurnal trunk shrinkage as a water stress indicator in plum trees," *Tree Physiol.*, vol. 26, pp. 303–311, 2006.

[33] C. J. Tucker, "Red and photographic infrared linear combinations for monitoring vegetation," *Remote Sens. Environ.*, vol. 8, pp. 127–150, 1979.

[34] J. A. Gamon *et al.*, "Relationships between NDVI, canopy structure, and photosynthesis in three Californian vegetation types," *Ecol. Appl.*, vol. 5, pp. 28–41, 1995.

[35] H. K. Lichtenthaler, A. A. Gitelson, and M. Lang, "Non-destructive determination of chlorophyll content of leaves of a green and an aurea mutant of tobacco by reflectance measurements," *J. Plant Physiol.*, vol. 148, pp. 483–493, 1996.

[36] B. N. Holben and C. O. Justice, "An examination of spectral band ratioing to reduce the topographic effect on remotely sensed data," *Int. J. Remote Sens.*, vol. 2, pp. 115–133, 1981.

[37] S. Delalieux, B. Somers, W. Verstraeten, J. A. N. Van Aardt, and P. Coppin, "Hyperspectral indices to diagnose leaf biotic stress of apple plants," *Int. J. Remote Sens.*, vol. 30, pp. 1887–1912, 2009.

[38] J. Gamon, J. Peñuelas, and C. B. Field, "A narrow-waveband spectral index that tracks diurnal changes in photosynthetic efficiency," *Remote Sens. Environ.*, vol. 41, pp. 35–44, 1992.

[39] R. Hernández-Clemente, R. Navarro-Cerrillo, L. Suárez, F. Morales, and P. J. Zarco-Tejada, "Assessing structural effects on PRI for stress detection in conifer forests," *Remote Sens. Environ.*, vol. 115, pp. 2360–2375, 2011.

[40] F. Thenot, M. Méthy, and T. Winkel, "The photochemical reflectance index (PRI) as a water-stress index," *Int. J. Remote Sens.*, vol. 23, pp. 5135–5139, 2002.

[41] T. Winkel, M. Méthy, and F. Thénot, "Radiation use efficiency, chlorophyll fluorescence, and reflectance indices associated with ontogenic changes in water-limited Chenopodium quinoa leaves," *Photosynthetica*, vol. 40, pp. 227–232, 2002.

[42] S. Z. Dobrowsky, J. C. Pushnik, P. J. Zarco-Tejada, and S. L. Ustin, "Simple reflectance indices track heat and water stress-induced changes in steady-state chlorophyll fluorescence at the canopy scale," *Remote Sens. Environ.*, vol. 97, pp. 403–414, 2005.

[43] S. Evain, J. Flexas, and I. Moya, "A new instrument for passive remote sensing: 2. Measurement of leaf and canopy reflectance changes at 531 nm and their relationship with photosynthesis and chlorophyll fluorescence," *Remote Sens. Environ.*, vol. 91, pp. 175–185, 2004.

[44] J. J. Peguero-Pina, F. Morales, J. Flexas, E. Gil-Pelegrín, and I. Moya, "Photochemistry, remotely sensed physiological reflectance index and de-epoxidation state of xanthophyll cycle in *Quercus coccifera* under intense drought," *Oecologia*, vol. 156, pp. 1–11, 2008.

[45] L. Suárez *et al.*, "Assessing canopy PRI for water stress detection with diurnal airborne imagery," *Remote Sens. Environ.*, vol. 112, pp. 560–575, 2008.

[46] J. Peñuelas, I. Filella, and J. A. Gamon, "Assessment of photosynthetic radiation use efficiency with spectral reflectance," *New Phytol.*, vol. 131, pp. 291–296, 1995.

[47] J. A. Gamon *et al.*, "Remote sensing of the xanthophyll cycle and chlorophyll fluorescence in sunflower leaves and canopies," *Oecologia*, vol. 85, pp. 1–7, 1990.

[48] B. Demmig-Adams, "Carotenoids and photoprotection: A role for the xanthopyll zeaxanthin," *Biochim. Biophys. Acta*, vol. 1020, pp. 1–24, 1990.

[49] J. Peñuelas and I. Filella, "Visible and near-infrared reflectance techniques for diagnosing plant physiological status," *Trends Plant Sci.*, vol. 3, pp. 151–156, 1998.

[50] J. Peñuelas and Y. Inoue, "Reflectance assessment of canopy CO2 uptake," *Int. J. Remote Sens.*, vol. 21, pp. 3353–3356, 2000.

[51] G. M. Trotter, D. Whitehead, and E. J. Pinkney, "The photochemical reflectance index as a measure of photosynthetic light use efficiency for plants with varying foliar nitrogen contents," *Int. J. Remote Sens.*, vol. 23, pp. 1207–1212, 2002.

[52] M. F. Garbulsky, J. Peñuelas, J. A. Gamon, Y. Inoue, and I. Filella, "The photochemical reflectance index (PRI) and the remote sensing of leaf, canopy and ecosystem radiation use efficiencies: A review and meta-analysis," *Remote Sens. Environ.*, vol. 115, pp. 281–297, 2011.

[53] J. B. Adams and A. R. Gillespie, *Remote Sensing of Landscapes with Spectral Images: A Physical Modeling Approach*. Cambridge, U.K.: Cambridge Univ. Press, 2006, 362p.

[54] D. A. Roberts, "Separating spectral mixtures of vegetation and soil," Ph.D. dissertation, Univ. Washington, Seattle, WA, USA, 1991, 180p.

[55] C. Borel and S. Gerstl, "Nonlinear spectral mixing models for vegetative and soil surfaces," *Remote Sens. Environ.*, vol. 47, pp. 403–416, 1994.

[56] J. B. Adams, M. O. Smith, and P. E. Johnson, "Spectral mixture modeling—A new analysis of rock and soil types at the Viking Lander-1 site," *J. Geophys. Res. Solid Earth Planets*, vol. 91, pp. 8098–8112, 1986.

[57] A. J. Elmore, J. F. Mustard, S. J. Manning, and D. B. Lobell, "Quantifying vegetation change in semiarid environments: Precision and accuracy of spectral mixture analysis and the normalized difference vegetation index," *Remote Sens. Environ.*, vol. 73, pp. 87–102, 2000.

[58] S. Tompkins, J. F. Mustard, C. M. Pieters, and D. W. Forsyth, "Optimization of endmembers for spectral mixture analysis," *Remote Sens. Environ.*, vol. 59, pp. 472–489, 1997.

[59] G. P. Asner and D. B. Lobell, "A biogeophysical approach for automated SWIR unmixing of soils and vegetation," *Remote Sens. Environ.*, vol. 74, pp. 99–112, 2000.

[60] D. A. Roberts *et al.*, "Mapping chaparral in the Santa Monica mountains using multiple endmember spectral mixture models," *Remote Sens. Environ.*, vol. 65, pp. 267–279, 1998.

[61] C. A. Bateson, G. P. Asner, and C. A. Wessman, "Endmember bundles: A new approach to incorporating endmember variability into spectral mixture analysis," *IEEE Trans. Geosci. Remote Sens.*, vol. 38, no. 2, pp. 1083–1094, Mar. 2000.

[62] A. Plaza, P. Martinez, R. Perez, and J. Plaza, "Spatial/spectral endmember extraction by multidimensional morphological operations," *IEEE Trans. Geosci. Remote Sens.*, vol. 40, no. 9, pp. 2025–2041, Sep. 2002.

[63] B. Somers, M. Zortea, A. Plaza, and G. P. Asner, "Automated extraction of image-based endmember bundles for improved spectral unmixing," *IEEE J. Sel. Topics Appl. Earth Observ. Remote Sens.*, vol. 5, no. 2, pp. 396–408, Apr. 2012.

[64] D. R. Peddle, F. G. Hall, and E. F. Ledrew, "Spectral mixture analysis and geometric-optical reflectance modeling of boreal forest biophysical structure," *Remote Sens. Environ.*, vol. 67, pp. 288–297, 1999.

[65] T. H. Painter, J. Dozier, D. A. Roberts, R. E. Davis, and R. O. Green, "Retrieval of subpixel snow-covered area and grain size from imaging spectrometer data," *Remote Sens. Environ.*, vol. 85, pp. 64–77, 2003.

[66] L. Tits *et al.*, "Hyperspectral shape-based unmixing to improve intra- and interclass variability for forest and agro-ecosystem monitoring," *ISPRS J. Photogramm. Remote Sens.*, vol. 74, pp. 163–174, 2012.

[67] A. Barducci and A. Mecocci, "Theoretical and experimental assesment of noise effects on least-squares spectral unmixing of hyperspectral images," *Opt. Eng.*, vol. 44, pp. 087008-1–087008-5, 2005.

[68] J. C. Harsayni and C. I. Chang, "Hyperspectral image classification and dimensionality reduction: An orthogonal subspace projection approach," *IEEE Trans. Geosci. Remote Sens.*, vol. 32, no. 4, pp. 779–785, Jul. 1994.

[69] B. Somers, G. P. Asner, L. Tits, and P. Coppin, "Endmember variability in spectral mixture analysis: A review," *Remote Sens. Environ.*, vol. 115, pp. 1603–1616, 2011.

[70] J. B. Adams, M. O. Smith, and A. R. Gillespie, "Imaging spectroscopy: Interpretation based on spectral mixture analysis," in *Remote Geochemical Analysis: Elements and Mineralogical Composition*, C. M. Pieters and P. Englert, Eds. Cambridge, U.K.: Cambridge Univ. Press, 1993, pp. 145–166.

[71] L. Bertels. (2013). *Colibri—The ENVI/IDL Code Library* [Online]. Available: http://sourceforge.net/projects/enviidlcodelibr/files/

[72] J.-L. Widlowski *et al.*, "The RAMI on-line model checker (ROMC): A web-based benchmarking facility for canopy reflectance models," *Remote Sens. Environ.*, vol. 112, pp. 1144–1150, 2008.

[73] J. Weber and J. Penn, "Creation and rendering of realistic trees," in *Proc. Siggraph*, 1995, pp. 119–128.

[74] S. Jacquemoud and F. Baret, "PROSPECT: A model of leaf optical properties spectra," *Remote Sens. Environ.*, vol. 34, pp. 75–91, 1990.

[75] J. Stuckens, S. Delalieux, R. Swennen, and P. Coppin, "A dorsiventral leaf radiative transfer model: Development, validation and improved model inversion techniques," *Remote Sens. Environ.*, vol. 113, pp. 2560–2573, 2009.

[76] B. Somers *et al.*, "Nonlinear hyperspectral mixture analysis for tree cover estimates in orchards," *Remote Sens. Environ.*, vol. 113, pp. 1183–1193, 2009.

[77] M. Pharr and G. Humphreys, *Physically Based Rendering. from Theory to Implementation*. San Mateo, CA, USA: Morgan Kaufmann, 2004.

[78] W. J. Kender, "Citrus," *HortScience*, vol. 38, pp. 1043–1047, 2003.

[79] C. Ballester, J. Castel, M. A. Jiménez-Bello, J. R. Castel, and D. S. Intrigliolo, "Thermographic measurement of canopy temperature is a useful tool for predicting water deficit effects on fruit weight in citrus trees," *Agric. Water Manage.*, vol. 122, pp. 1–6, 2013.

[80] C. Ballester, J. Castel, D. S. Intrigliolo, and J. R. Castel, "Response of Clementina de Nules citrus trees to summer deficit irrigation. Yield components and fruit composition," *Agric. Water Manage.*, vol. 98, pp. 1027–1032, 2011.

[81] J. Biesemans *et al.*, "Image processing workflows for airborne remote sensing," in *Proc. 5th EARSEL Workshop Imag. Spectrosc.*, Bruges, Belgium, Apr. 23–25, 2007, pp. 1–14.

[82] D. R. Peddle and M. Smith, "Spectral mixture analysis of agricultural crops: Endmember validation and biophysical estimation in potato plots," *Int. J. Remote Sens.*, vol. 26, pp. 4959–4979, 2005.

[83] S. Jacquemoud *et al.*, "Estimating leaf biochemistry using the PROSPECT leaf optical properties model," *Remote Sens. Environ.*, vol. 56, pp. 194–202, 1996.

[84] J. B. Feret, C. François, and G. P. Asner, "PROSPECT-4 and 5: Advances in the leaf optical properties model separating photosynthetic pigments," *Remote Sens. Environ.*, vol. 112, pp. 3030–3043, 2008.

[85] P. J. Zarco-Tejada, J. R. Miller, A. Morales, A. Berjón, and J. Agüera, "Hyperspectral indices and model simulation for chlorophyll estimation in open-canopy tree crops," *Remote Sens. Environ.*, vol. 90, pp. 463–476, 2004.

[86] P. J. Curran, "Remote sensing of foliar chemistry," *Remote Sens. Environ.*, vol. 30, pp. 271–278, 1989.

[87] F. Zagolski *et al.*, "Forest canopy chemistry with high spectral resolution remote sensing," *Int. J. Remote Sens.*, vol. 17, pp. 1107–1128, 1996.

[88] R. D. Jackson, D. B. Idso, R. J. Reginato, and P. J. Pinter, Jr., "Canopy temperature as a crop water stress indicator," *Water Resour. Res.*, vol. 17, pp. 1133–1138, 1981.

[89] Y. Cohen, V. Alchanatis, M. Meron, Y. Saranga, and J. Tsipris, "Estimation of leaf potential by thermal imagery and spatial analysis," *J. Exp. Bot.*, vol. 56, pp. 1843–1852, 2005.

[90] S. B. Idso, R. D. Jackson, and B. J. Reginato, "Extending the "degree day" concept of phenological development to include water stress effects," *Ecology*, vol. 59, pp. 431–433, 1978.

[91] I. Leinonen and H. G. Jones, "Combining thermal and visible imagery for stimulating canopy temperature and identifying plant stress," *J. Exp. Bot.*, vol. 55, pp. 1423–1431, 2004.

[92] M. Möller *et al.*, "Use of thermal and visible imagery for estimating crop water status of irrigated grapevine," *J. Exp. Bot.*, vol. 58, pp. 827–838, 2007.

[93] G. Sepulcre-Cantó *et al.*, "Within-field thermal variability detection as function of water stress in Olea europaea L. orchards with high spatial remote sensing imagery," *Agric. Forest Meteorol.*, vol. 136, pp. 31–44, 2006.
[94] G. Sepulcre-Cantó *et al.*, "Monitoring yield and fruit quality parameters in open-canopy tree crops under water stress. Implications for ASTER," *Remote Sens. Environ.*, vol. 107, pp. 455–470, 2007.
[95] D. F. Wanjura, S. C. Maas, D. R. Winslow, and D. R. Upchurch, "Scanned and spot measured canopy temperatures of cotton and corn," *Comput. Electron. Agric.*, vol. 44, pp. 33–48, 2004.
[96] J. M. Bioucas-Dias *et al.*, "Hyperspectral unmixing overview: Geometrical, statistical, and sparse regression-based approaches," *IEEE J. Sel. Topics Appl. Earth Observ. Remote Sens.*, vol. 5, no. 2, pp. 354–379, Apr. 2012.
[97] G. A. Licciardi and F. Del Frate, "Pixel unmixing in hyperspectral data by means of neural networks," *IEEE Trans.Geosci. Remote Sens.*, vol. 49, no. 11, pp. 4163–4172, Nov. 2011.

Stephanie Delalieux received the Ph.D. degree in applied bioscience and engineering from the Katholieke Universiteit Leuven, Leuven, Belgium, in 2009.

She is currently a Senior Researcher with the Remote Sensing Division, Flemish Institute for Technological Research (VITO), Mol, Belgium. Her research interests include the use and application of high spectral, high spatial and/or, high temporal resolution remote sensing data, and processing for precision agriculture and biodiversity applications.

Pablo J. Zarco-Tejada received the degree in agricultural engineering from the School of Agricultural Engineering and Forestry, University of Córdoba, Spain, the M.Sc. degree in remote sensing from the University of Dundee, Scotland, U.K., and the Ph.D. degree in earth and space science from York University, Toronto, ON, Canada.

He has been a contract Faculty Member for remote sensing with the University of California, Davis, CA, USA. He leads the Laboratory for Research Methods in Quantitative Remote Sensing (QuantaLab), Institute for Sustainable Agriculture (IAS), National Research Council (CSIC), Spain. His research interests include vegetation stress detection, physiological condition, and precision agriculture using manned and unmanned aerial vehicles.

Laurent Tits received the M.Sc. and Ph.D. degrees in bioscience engineering in land and forest management from the KU Leuven, Leuven, Belgium, in 2009 and 2013, respectively.

Since 2010, he has been a Research Assistant with the Geomatics Engineering Group, Department of Biosystems, KU Leuven. His research interests include hyperspectral as well as thermal remote sensing in vegetative systems, spectral, and thermal mixture analysis.

Miguel Ángel Jiménez Bello received the M.Sc. degree in geo-information sciences from Wageningen University, Wageningen, The Netherlands, in 2002, and the Ph.D. degree in hydraulics engineering from the Polytechnic University of Valencia, Valencia, Spain, in 2008.

He is currently a Researcher with the Research Institute of Water and Environmental Engineering (IIAMA) and an Assistant Professor in hydraulics with the Polytechnic University of Valencia. He developed his activity at the Agriculture Valencia Research (IVIA) to determine crop water requirements and stress by means of remote sensing tools. His research interests include irrigation management from the hydraulic and agronomic point of view.

Diego S. Intrigliolo received the Ph.D. degree in agriculture engineering, Polytechnic University of Valencia, Valencia, Spain (2005) with a Postdoctoral stay at Cornell University, Ithaca, NY, USA (2008).

He is currently a Research Associate with the Valencia Institute of Agriculture Research (IVIA), Spain. His research interests include the use of plant and soil water status data for scheduling irrigation and the quantification of woody perennial crop responses to the irrigation regime.

Ben Somers was born in Leuven, Belgium on September 13, 1982. He received the M.Sc. and Ph.D. degrees in bioscience engineering in land and forest management from the Katholieke Universiteit Leuven (KULeuven), Leuven, Belgium, in 2005 and 2009, respectively.

In 2010, he was the Research Associate with the Geomatics Engineering Group, KULeuven. Between 2011 and 2013, he was the Researcher with the Remote Sensing Division, Flemish Institute for Technological Research (VITO), Mol, Belgium. In October 2013, he started as an Assistant Professor (tenure track position) with the Division of Forest, Nature and Landscape, Department of Earth and Environmental Sciences of the KULeuven. He is experienced in the design and integration of state-of-the-art remote sensing techniques to study the impact of disturbance processes (nutrient deficiencies, pests and diseases, invasive exotic species, climate change) on the functioning of terrestrial ecosystems. His research interests include fostering the use and application of remote sensing in support of sustainable management of (semi)natural and urban environments.